NASA CR-144978

FLOW RESEARCH, INC.

NUMERICAL SIMULATION OF TURBULENT JET NOISE - PART II

by

Ralph W. Metcalfe

and

Steven A. Orszag

Prepared under Contract No. NAS1-12870

Flow Research, Inc.

Kent, Washington

for

NATIONAL AERONAUTICS AND SPACE ADMINISTRATION

February 1976

Flow Research Report No. 62

N76-30921

Unclas
49532
G3/71

(NASA-CR-144978) NUMERICAL SIMULATION OF TURBULENT JET NOISE, PART 2 (Flow Research, Inc., Kent, Wash.) 25 p HC $3.50 CSCL 20A

AUG 1976
RECEIVED
NASA STI FACILITY
INPUT BRANCH

HEADQUARTERS: 1819 South Central Ave., Kent, WA. 98031
LOS ANGELES DIVISION: Suite 1004, 9841 Airport Blvd., Los Angeles, CA. 90045 • (213) 641-4691
PRINCETON COMBUSTION LABS: P.O. Box 297, Plainsboro, N.J. 08536 • (609) 452-8060
EUROPE: 59 Burton Rd., Bletchley, Milton Keynes, MK2 2BL England • MK0908 71571/71572 • Telex 826971

Table of Contents

		Page
	Table of Contents	i
1.	Introduction	1
2.	Flow Model and Numerical Methods	2
3.	Radiated Sound Field From a Turbulent Jet	5
4.	Numerical Methods	10
	4.1 Semi-Implicit Treatment of the Nonlinear Terms	10
	4.2 Isentropic Compressible Flow	11
	4.3 Nonlinear Eddy Viscosity	11
5.	Summary	13
	References	14
	Figures	15

1. Introduction

In Part I of this work (Metcalfe and Orszag, 1975) the numerical simulation of detailed turbulent flow fields was reported. Here in Part II, these jet flow fields were used to study the radiated sound field, and in addition, to extend and test the capabilities of the turbulent jet simulation codes. The goal of this work is to complement the theoretical and experimental research programs of the NASA Langley Research Center on aerodynamic noise generation. The computer simulations of Metcalfe and Orszag (1975) provide a variety of data that are very difficult or even impossible to obtain by other methods.

The principal new result of the present work is the computation of the radiated sound field from a turbulent jet. In addition, the computer codes have been extended to account for the effects of compressibility and eddy viscosity, and the treatment of the nonlinear terms of the Navier-Stokes equations has been modified so that they can be computed in a semi-implicit way. In Sec. 2 of this report is a summary of the flow model and a description of the numerical methods used for its solution. In Sec. 3, calculations of the radiated sound field are reported. In Sec. 4, the extensions that have been made to the fundamental dynamical codes are described. Finally, in Sec. 5, the current state-of-the-art for computer simulation of turbulent jet noise is summarized.

2. Flow Model and Numerical Methods

The basic flow model to determine the jet flow field is based on the Navier-Stokes equations for incompressible flow. At low Mach number, the acoustic components of the flow field are only weakly coupled to the shear (rotational) components so that the flow field can be determined to a good approximation by neglecting the weakly excited acoustic field. After the rotational flow is determined by numerical integration of the Navier-Stokes equations, the acoustic field can be determined by Lighthill's perturbation procedure from the quadrupole moments of the flow field. The latter calculation is reported in Sec. 3.

The Navier-Stokes equations for incompressible flow are

$$\frac{\partial \vec{v}}{\partial t} + \vec{v} \cdot \vec{\nabla} \vec{v} = -\vec{\nabla} p + \nu \nabla^2 \vec{v} \qquad (1)$$

$$\vec{\nabla} \cdot \vec{v} = 0 \qquad (2)$$

where $\vec{v}(\vec{x},t)$ is the velocity at $\vec{x},t$, $p(\vec{x},t)$ is the pressure, ν is the kinematic viscosity, and the density ρ is assumed to be 1. The numerical simulation of a turbulent jet flow field using (1)-(2) is beset with two major difficulties: first, the required computer resolution to calculate a high Reynolds number flow accurately is enormous; and, second, the boundary conditions that must be imposed to simulate a jet are very difficult to impose. Because of these problems, the flow model was further simplified as discussed below. Laboratory experiments, such as those of Liu and Maestrello (1974) have determined the large-scale mean-flow characteristics accurately, so these flow characteristics are reasonably chosen to be <u>input</u> to the numerical computations. The numerical computations are then used to predict the quadrupole moment distribution given the large-scale mean-flow characteristics of the turbulence. Since the quadrupole source terms are dominated by small-scale motions and since the small-scale motions of turbulence are determined by the <u>local</u> large-scale characteristics, it follows that the acoustic source terms can be effectively determined by isolating a small local section of the jet. This avoids the two difficulties mentioned above. First, because a small section of the jet is being simulated, it is not necessary to simulate at one time all twenty or

so jet diameters in the downstream direction that contribute to the noise generation by the jet. Second, within each local section of the jet, it is most reasonable to impose periodic boundary conditions because only local turbulence is being studied. The turbulence within each jet section is, however, strongly affected by the mean flow characteristics that are imposed, the latter being those appropriate to the jet section being simulated.

In summary, the flow model involves the isolation of a local section of the jet, imposition of periodic boundary conditions, maintenance for all time of the experimentally observed mean-flow characteristics, and numerical integration of the Navier-Stokes equations in time until a statistically steady state is achieved. After evolving the flow in this way, the quadrupole moments are extracted from the statistically steady turbulent state and used in the manner described in Sec. 3 to determine the radiated acoustic field.

In accord with this flow model, the velocity field is expressed as

$$\vec{v}(\vec{x},t) = \vec{V}(\vec{x}) + \vec{v}'(\vec{x},t) \tag{3}$$

where $\vec{V}$ is the imposed mean velocity (constant for all time) and $\vec{v}'$ is the fluctuating velocity. At all downstream locations the mean velocity $\vec{V}$ is of the form

$$\vec{V}(\vec{x}) = U(r)\hat{x}_1 \tag{4}$$

where $\hat{x}_1$ is a unit vector in the x_1 direction, r is the distance from the jet axis, and $U(r)$ is the experimentally determined profile (see Fig. 1).

The Navier-Stokes equations are integrated by expressing the velocity field in terms of (special) Fourier series of the form

$$\vec{v}(\vec{x},t) = \sum_{|k_1|<k_1} \sum_{|k_2|<k_2} \sum_{|k_3|<k_3} \vec{u}(\vec{k},t)\exp(2\pi i\vec{k}\cdot\vec{x}) \ . \tag{5}$$

In fact, the Fourier expansion (5) is specialized so that the velocity field that is represented has zero stress boundary conditions imposed on the x_2 and x_3 boundaries; these latter boundary conditions are a convenient way of handling the potential flow outside the jet without imposition of complicated entrainment boundary conditions. Altogether, 32,768 <u>independent</u> Fourier

components are used to represent each component of the velocity field, so that about 10^5 independent data are used to represent the complete flow field. The numerical solution of the Navier-Stokes equations proceeds by using the Fourier representation (5) together with the fast Fourier transform to allow efficient evaluation of derivatives appearing in the equations. Time-stepping is performed by a fractional step technique in which leapfrog differencing is used to evaluate the nonlinear terms in (1) and Crank-Nicolson implicit differencing is used to evaluate the viscous terms. A semi-implicit scheme for the evaluation of the nonlinear terms is described in Sec. 4.

The mean velocity profile $U(r)$ in (5) was chosen to correspond to the experimentally determined profile of an axisymmetric cold subsonic jet, as parametrized by Maestrello, et al. (1974). This velocity profile is plotted in Fig. 2 at three downstream locations, 4, 8, and 12 jet diameters downstream. Also, the mean turbulent intensities and their radial variation is imposed following the parametrization of Liu and Maestrello (1974); the radial variation of the rms turbulent intensity at 4, 8, and 12 jet diameters downstream is plotted in Fig. 3.

In order to give perspective on the degree of complication of the velocity field in these calculations, in Figs. 4 and 5 contours of the x_1 component of the velocity field for the simulation performed at 12 diameters downstream from the jet exit are plotted. In Fig. 4, the contours of v_1 are plotted in the x_2-x_3 plane at $x_1 = 12$ diameters at $t = 0.32$, after a statistically steady state has been achieved. In Fig. 5, the contours of v_1 are plotted at the same time of evolution in the x_1-x_3 plane passing through the center of the jet.

3. Radiated Sound Field From a Turbulent Jet

According to Lighthill's theory (1952) of aerodynamic sound generation, the sound radiated by turbulence satisfies the inhomogeneous wave equation

$$\frac{\partial^2 \rho}{\partial t^2} - c^2 \nabla^2 \rho = \frac{\partial^2}{\partial x_i \partial x_j} T_{ij} \equiv Q(\vec{x},t) \tag{6}$$

where

$$T_{ij} = \rho_o v_i v_j \, . \tag{7}$$

Here $\rho_o = 1$ is the unperturbed (non-acoustic) density in the flow field while $\rho(\vec{x},t)$ is the fluctuating density field, i.e., the radiated acoustic field. The solution to (6) that satisfies the outgoing radiation condition at ∞ is

$$\rho(\vec{x},t) = \frac{1}{4\pi c^2} \int Q\left(\vec{y}, t - \frac{|\vec{x}-\vec{y}|}{c}\right) \frac{d\vec{y}}{|\vec{x}-\vec{y}|} \, , \tag{8}$$

which is Lighthill's integral solution for the radiated sound field.

In the work reported here, the Lighthill integral solution (8) has been used to determine acoustic radiation characteristics similar to those measured by Maestrello (1973) in a careful analysis of the radiation patterns of a turbulent jet. Maestrello measured the correlation coefficient of derivatives of the pressure:

$$R_{\nabla\rho,\nabla p}(\vec{x},t;\vec{x}+\vec{y},t+\tau) = \overline{\frac{\partial p}{\partial r}(\vec{x},t) \, \frac{\partial p}{\partial r}(\vec{x}+\vec{y},t+\tau)} \tag{9}$$

where the derivatives are taken along the radial direction normal to the jet axis and the overbar indicates average. Maestrello reported extensive measurements of $R_{\nabla p,\nabla p}$ for various separation vectors $\vec{y}$ and time shifts τ.

It is possible to use the Lighthill integral (8) to obtain an explicit expression for $R_{\nabla p,\nabla p}$ in terms of the source distribution T_{ij}. To do this, it must be noted that $\nabla p = c^2 \nabla \rho$ in the acoustic field so that $R_{\nabla p,\nabla p}$ can be computed by correlating gradients of (8). In particular, it follows that

$$R_{\nabla p,\nabla p}(\vec{x},t;\vec{x}+\vec{y},t+\tau)$$

$$= \left(\frac{1}{4\pi}\right)^2 \left(\frac{\partial}{\partial r}\right)_x \left(\frac{\partial}{\partial r}\right)_{x+y} \iint \overline{Q\left(\vec{y}_1, t - \frac{|\vec{x}-\vec{y}_1|}{c}\right) Q\left(\vec{y}_2, t+\tau - \frac{|\vec{x}+\vec{y}-\vec{y}_2|}{c}\right)}$$

$$\times \frac{1}{|\vec{x}-\vec{y}_1|\,|\vec{x}+\vec{y}-\vec{y}_2|}\, d\vec{y}_1\, d\vec{y}_2 \quad . \tag{10}$$

Expression (10) is used to obtain the principal results reported below.

Before proceeding to report these results, a simple argument can be made to establish the essential features of the correlation (10). Assume that jet turbulence has a local spatial correlation scale L and a local time correlation scale T. Also assume that the local field of turbulence is convected at the large speed U of the jet past a fixed frame of reference. In that case the integrand of (10) differs significantly from $\overline{T_{ij}(y_1,t_1)\, T_{kl}(y_2,t_2)}$, i.e., the uncorrelated average of the source terms, only if $|y_1 - y_2| \leq L$ and

$$c\tau + \frac{\xi D}{R} < cT$$

where D is the jet diameter. Assume $R = |\vec{x}| = |\vec{x}+\vec{y}| >> D$ so that the two observation points lie on the same cylindrical sleeve around the turbulent jet and both points lie in the far field of the radiation pattern. Here $\xi = |\vec{y}|$ is the distance between the two observation points. If it is further assumed that the turbulence scale L is a constant fraction of the local jet diameter D, some interesting scaling conclusions may be drawn. First, the correlation (10) should decay to zero in a time scale proportional to $T(1 - c\theta M)$ where c is a constant, θ is the angular separation between $\vec{x}$ and $\vec{x}+\vec{y}$ ($\theta = \xi/R$, where $R = |\vec{x}+\vec{y}| = |\vec{x}|$), and $M = U/c$ is the local jet Mach number. Second, equal time correlations $\tau = 0$ should decay to zero over a distance

$$\theta \propto \frac{1}{M} \tag{11}$$

where θ is the angular separation of $\vec{x}$ and $\vec{x} + \vec{y}$. It will be interesting to determine whether the correlations determined experimentally behave according to (11) in the far field. It seems that the data of Maestrello (1973) does not yet provide sufficient information to test (11). Equation (11) has not yet been tested against the present numerical data, although it is certainly possible to do this. However, it seems that (11) is built into the present numerical scheme automatically because (10) is assumed to be true. Equation (11) follows from (10), as shown above, by very crude turbulence theory arguments, which seem to be well satisfied by the numerical simulations.

The experimental configuration for Maestrello's (1973) measurements was a 213 m/s cold jet with exit diameter 0.0625 m. Maestrello made measurements at a number of downstream stations as illustrated in Fig. 6. Here, the numerical simulation of his results for station 5 (for which the most data is available) has been attempted. Station 5 of the laboratory experiment is at 7.42 diameters downstream from the jet exit, and the numerical simulation consists of isolating a jet section at 8 diameters downstream. The acoustic field is then determined along a cylindrical sleeve whose axis is aligned with the jet axis and whose radius is 5 local jet diameters (radius 46 cm).

The numerical computations of $R_{\nabla p, \nabla p}(\xi, \tau)$, where ξ is the circumferential separation of two points on the measuring cylinder at the same axial distance downstream and τ is the time separation between the measurements, were performed as follows. First, the statistically steady turbulent flow at 8 jet diameters downstream was calculated as described in Sec. 2. The computational domain extended over three jet diameters in the downstream direction. Second, the quadrupole source distributions resulting from these calculations was substituted into the Lighthill integral (8) and the acoustic field was determined over the whole cylindrical sleeve about the jet. In performing the latter computation, the local Mach number was assumed to be the same as for the 213 m/s jet studied by Maestrello. It was also assumed that no significant contributions to the acoustic field come from regions of the jet more distant than the present computational domain, i.e., more distant than 3 jet diameters from the local position in the axial direction. After finding the acoustic field in this way, the correlation $R_{\nabla p, \nabla p}(\xi, \tau)$ was found

by averaging the results for all available points with the given space and time separations over the cylindrical sleeve (this average being justified by the axisymmetry of the flow) and over time (this average being justified by the statistical stationarity of the flow).

The results for the correlation $R_{\nabla p, \nabla p}(\xi, \tau)$ at station 5 are shown in Fig. 7. These results bear some striking similarity to Maestrello's results, but they are also in substantial disagreement. The general structure of the correlations is very similar to those measured by Maestrello (see his Fig. 14 reproduced here as Fig. 8). The correlations have significant negative regions; they decay to zero rapidly with increasing ξ and τ. However, there are some significant discrepancies. First, Maestrello's data does not show the symmetry of the numerical data plotted in Fig. 7; this symmetry is built into the numerical experiments to high accuracy because of the way the average $R_{\nabla p, \nabla p}$ is obtained. The numerical data do not show any displacement of the correlation peak as a function of ξ. Also, the time scale over which the numerical correlations decay to zero is about twice as long as the time scale over which the experimental data decays to zero.

There are several possible explanations for these discrepancies between the numerical and laboratory data. If it is assumed that there are no systematic experimental errors (which seems fully justified by recent repetitions of the experiments), one must conclude that the discrepancies are due to either: (i) a Reynolds number effect (since the Reynolds number of the simulations is an order of magnitude less than that of the experiments); (ii) the effect of the simplified boundary conditions in the flow model; (iii) an effect of compressibility; (iv) an effect of departures from statistical stationarity in the numerical simulations; (v) an effect of lack of computer resolution in performing the averages or integrals; or (vi) a measure of the inaccuracy of Lighthill's integral (8) for the radiated sound. Of all these possibilities, it is believed that the most likely causes of the error are (ii), (iv), (i), (vi), (v), (iii), in order of decreasing likelihood. However, it is not possible to state with certainty at this time the precise cause of the quantitative discrepancies.

In summary, the qualitative nature of the radiated sound field bears good relation to the experiments of Maestrello (1973), but there is some quantitative disagreement. Nevertheless, there is ample ground

for believing that a high-resolution numerical experiment, say one performed on an advanced scientific computer like the CDC STAR, will give both good quantitative and qualitative agreement with laboratory (and field) experiment.

4. Numerical Methods

Three major modifications have been made to the numerical methods used by Metcalfe and Orszag (1975) in order to improve the flow model for turbulent jet flow. These improvements are: (i) a semi-implicit treatment of the nonlinear terms; (ii) modification of the incompressible flow program to treat isentropic compressible flow; and (iii) inclusion of nonlinear eddy viscosity in the code. These modifications will now be discussed in order.

4.1 Semi-Implicit Treatment of the Nonlinear Terms

The most severe restriction on the size of time steps in the numerical calculations reported by Metcalfe and Orszag (1975) is due to the convective stability restrictions originating from the large axial jet velocity: if the maximum jet velocity is U and the axial grid (or Fourier) resolution is Δx, then time steps in an explicit time integration scheme are restricted by $\Delta t < \Delta x/U$.

Metcalfe and Orszag (1975) have developed a method that significantly relaxes the above time-stepping restriction to $\Delta t < \Delta x/v_{rms}$ where v_{rms} is the rms turbulent velocity. Since $v_{rms} \sim U/5$, the new time stepping scheme allows time steps that are several times large than those without the semi-implicit scheme.

The technique for implementing the semi-implicit scheme is to split the total velocity into two parts:

$$\vec{v} = \vec{V} + \vec{v}' \tag{12}$$

where $\vec{V}$ is the mean axial flow and $\vec{v}'$ is the fluctuating velocity. The nonlinear term representing the advection of $\vec{v}$ by $\vec{V}$ is treated implicitly, while the nonlinear term involving the advection of $\vec{v}$ by $\vec{v}'$ is treated explicitly. Thus, the semi-implicit treatment of the nonlinear terms involves the solution of the implicit equation

$$\frac{\partial \vec{v}}{\partial t} + V(r) \frac{\partial \vec{v}}{\partial x_1} = \vec{f} \tag{13}$$

in which V and f are known. The implicit solution of (13) is easily done in the spectral representation in x_1 because the mean velocity V is independent of x_1 in the flow model. Thus, if k is the Fourier variable

conjugate to the coordinate x_1, the solution to (13) using Crank-Nicolson time-differencing is simply

$$\vec{v}(k,x_2,x_3,t+\Delta t) = \left[\vec{v}(k,x_2,x_3,t) + \Delta t\vec{f}(t+\tfrac{1}{2}\Delta t) - \tfrac{1}{2}ikV(r)\Delta t\vec{v}(k,x_2,x_3,t)\right] /$$

$$(1 + \tfrac{1}{2} ik\, V(r)\Delta t) \ . \qquad (14)$$

4.2 Isentropic Compressible Flow

The compressible flow equations for isentropic flow in a polytropic gas are

$$\rho\left[\frac{\partial\vec{v}}{\partial t} + \vec{v}\cdot\nabla\vec{v}\right] = -\vec{\nabla}p + \nu_1\nabla^2\vec{v} + \nu_2\,\vec{\nabla}(\vec{\nabla}\cdot\vec{v}) \qquad (15)$$

$$\frac{\partial\rho}{\partial t} + \vec{v}\cdot\vec{\nabla}\rho + \rho\vec{\nabla}\cdot\vec{v} = 0 \qquad (16)$$

$$p = K\rho^{\gamma} \ . \qquad (17)$$

The method of solution (15)-(17) is very similar to that of (1)-(2). All flow variables are expanded in the Fourier series (5), which is used to effect the evaluation of derivatives appearing in (15)-(17). The necessary modifications in the codes have been made to implement simulations with $32 \times 32 \times 32$ Fourier components used to resolve each of the flow variables. The running time is 8s per time step.

Preliminary studies have been made of another modification in this compressible flow code, viz. the inclusion of non-isentropic flow effects. Gottlieb and Orszag (1976) nave studied the accuracy and efficiency of the spectral methods used in the jet flow simulations for the calculation of highly compressible flows with shocks. The results of these calculations are encouraging in the sense that shocks can be resolved accurately with very few dynamical degrees of freedom if localized dissipation is imposed in the neighborhood of the shock.

4.3 Nonlinear Eddy Viscosity

The codes developed by Metcalfe and Orszag (1975) have been modified to include the effect of subgrid scale turbulence by means of a nonlinear eddy

viscosity similar to that employed by Deardorff (1970) and others. Deardorff (1970) has modeled subgrid scale effects by including a term with an eddy coefficient proportional to the local velocity deformation. In the simulations reported here, subgrid scale turbulence has been modeled by adding a term to equation (1) that is proportional to the root mean square vorticity. The simulation of the jet flow at 8 diameters downstream from the jet exit has been repeated, using this modified form of energy dissipation. The results of this simulation are quite striking. When velocity contours of the two simulations are compared there is no noticeable difference at the computation time of 0.032, which is in the interval of times used for the calculations reported in Sec. 3. It is concluded that there is no significant Reynolds number effect on the velocity fields used for the numerical simulations. However, there may still be a Reynolds number effect on the quadruple moment fields used for the acoustic source field; comparisons of the simulations of Metcalfe and Orszag (1975) with the simulation made using the nonlinear eddy viscosity are inconclusive on this latter point. The Reynolds number variation of the quadrupole moment fields are still a matter of research interest, which will be studied with the use of these codes.

5. Summary

This report has discussed the progress in the numerical simulation of jet turbulence and aerodynamic noise radiated by jets. It is believed that a significant breakthrough in the numerical simulation of a turbulent jet's noise radiation pattern has been achieved. The results plotted in Fig. 7 show good qualitative agreement with those determined experimentally (plotted in Fig. 8) despite the limited computer resolution of the present computations. This is not a trivial accomplishment; for example, if a ring vortex model is used to simulate the quadrupole moment field of a turbulent jet, the radiation field is axisymmetric and perfectly correlated around the jet. There is no decorrelation with increasing ξ in a ring vortex model. Nevertheless, solution of the three-dimensional Navier-Stokes equations, even with the limited flow model presented here, gives striking confirmation of the experimental results. It should be expected that improvements in the flow model and increased computer resolution will improve the quantitative agreement between numerical and laboratory and field experiments.

Finally, in Sec. 4 the improvements made in the flow model and in the numerical techniques for its solution have been summarized. As mentioned earlier, the principal area for further improvement involves the treatment of the boundary conditions. However, improvements of the treatment of the boundary conditions will require substantially more computer resolution than presently available. It will not be possible to isolate a small section of the jet to be simulated independently of other sections of the jet; it will not be possible to neglect effects of entrainment of fluid from infinity or effects at the jet exit. It seems that such substantial improvement of the flow model must await the next generation of powerful computers.

References

Deardorff, J. W. (1970) "A Numerical Study of Three-Dimensional Turbulent Channel Flow at Large Reynolds Numbers," J. Fluid Mech. 41, 453-480.

Gottlieb, D. and Orszag, S. A. (1976) "Spectral Methods for Compressible Flow Problems," in preparation.

Lighthill, M. J. (1952) "On Sound Generated Aerodynamically, I. General Theory," Proc. Roy. Soc. A 211, 564-587.

Liu, C. H. and Maestrello, L. (1974) "Propagation of Sound Through a Real Jet Flowfield," AIAA Paper No. 74-5.

Maestrello, L. (1973) "On the Relationship Between Acoustic Energy Density Flux Near the Jet and Far Field Acoustic Intensity," AIAA Paper 73-988.

Maestrello, L., Liu, C. H. and Gunzburger, M. D. (1974) "Sound Propagation Through a Real Jet Flowfield With Scattering Due to Interaction With Turbulence," AIAA Paper No. 74-551.

Metcalfe, R. W. and Orszag, S. A. (1975) "Numerical Simulation of Turbulent Jet Noise - Part I.," NASA Report CR-132693. (This paper is referred to as Part I in the text.)

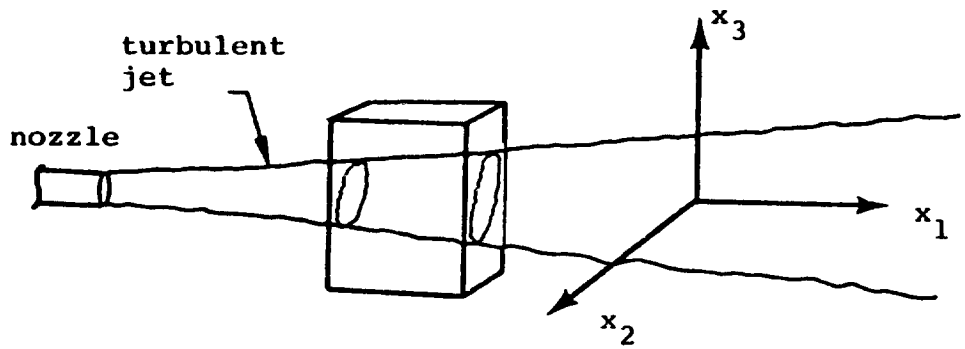

Figure 1. Schematic diagram showing the section of the jet being modeled in numerical simulations. The box indicates the computational region.

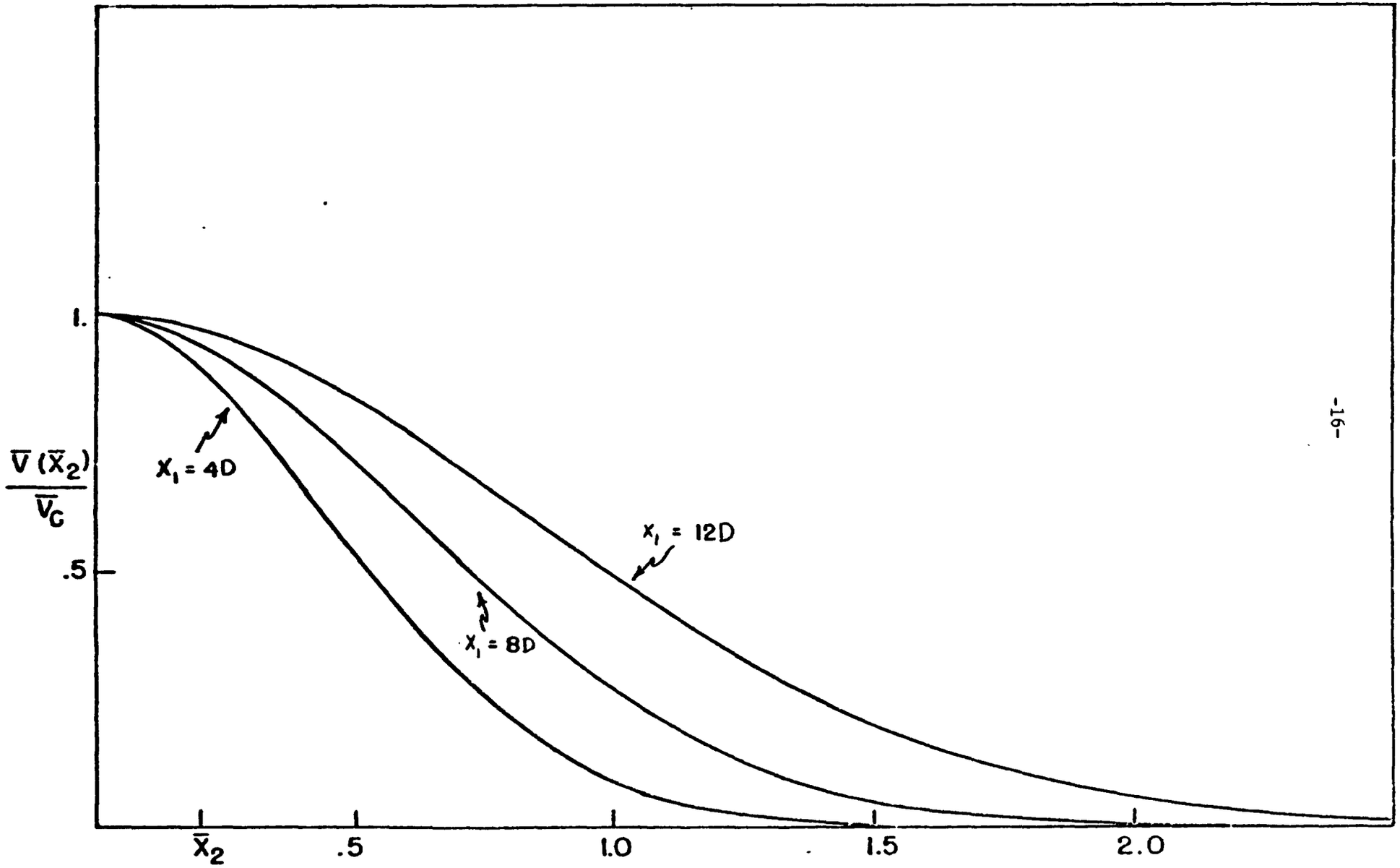

Figure 2. Initial mean velocity profiles at three downstream positions.

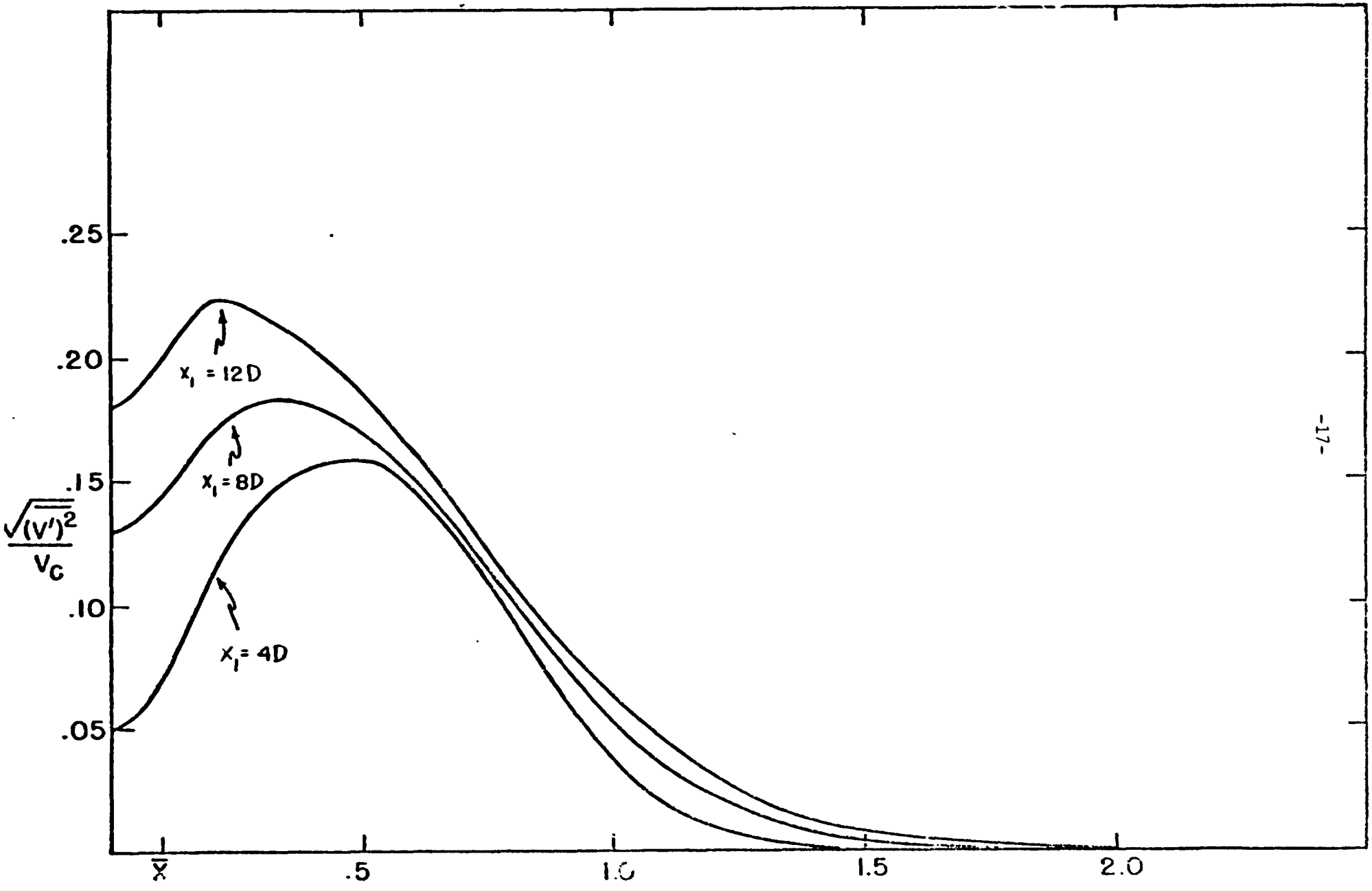

Figure 3. Root mean square turbulent intensities at three downstream positions.

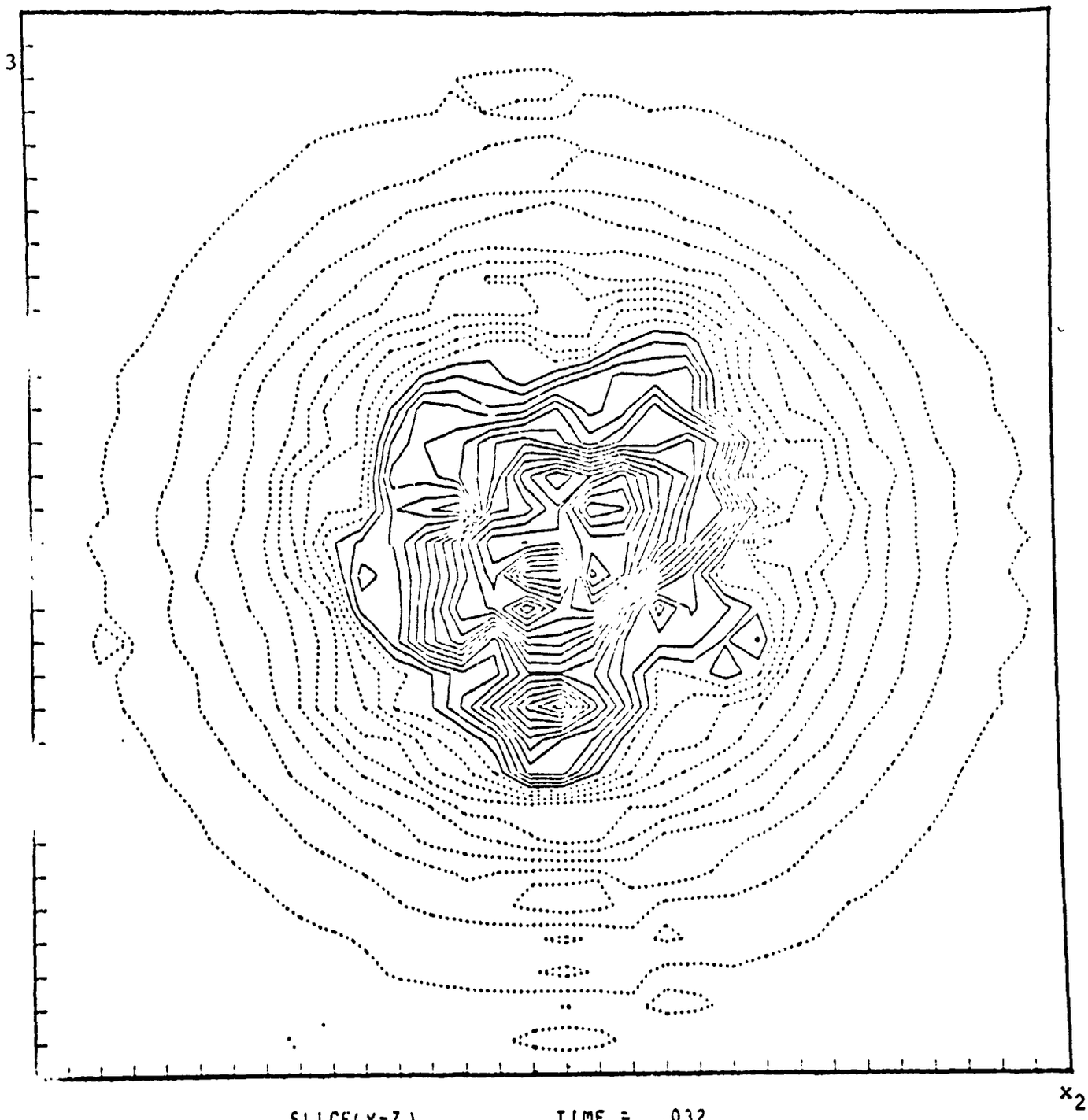

Figure 4. Contour plot of $v_1(x_1,x_2,x_3)$ in the plane $x_1=\frac{1}{2}L$ at $\bar{X}$ = 12 diameters downstream from the jet exit. Here t = .032s is the time of evolution.

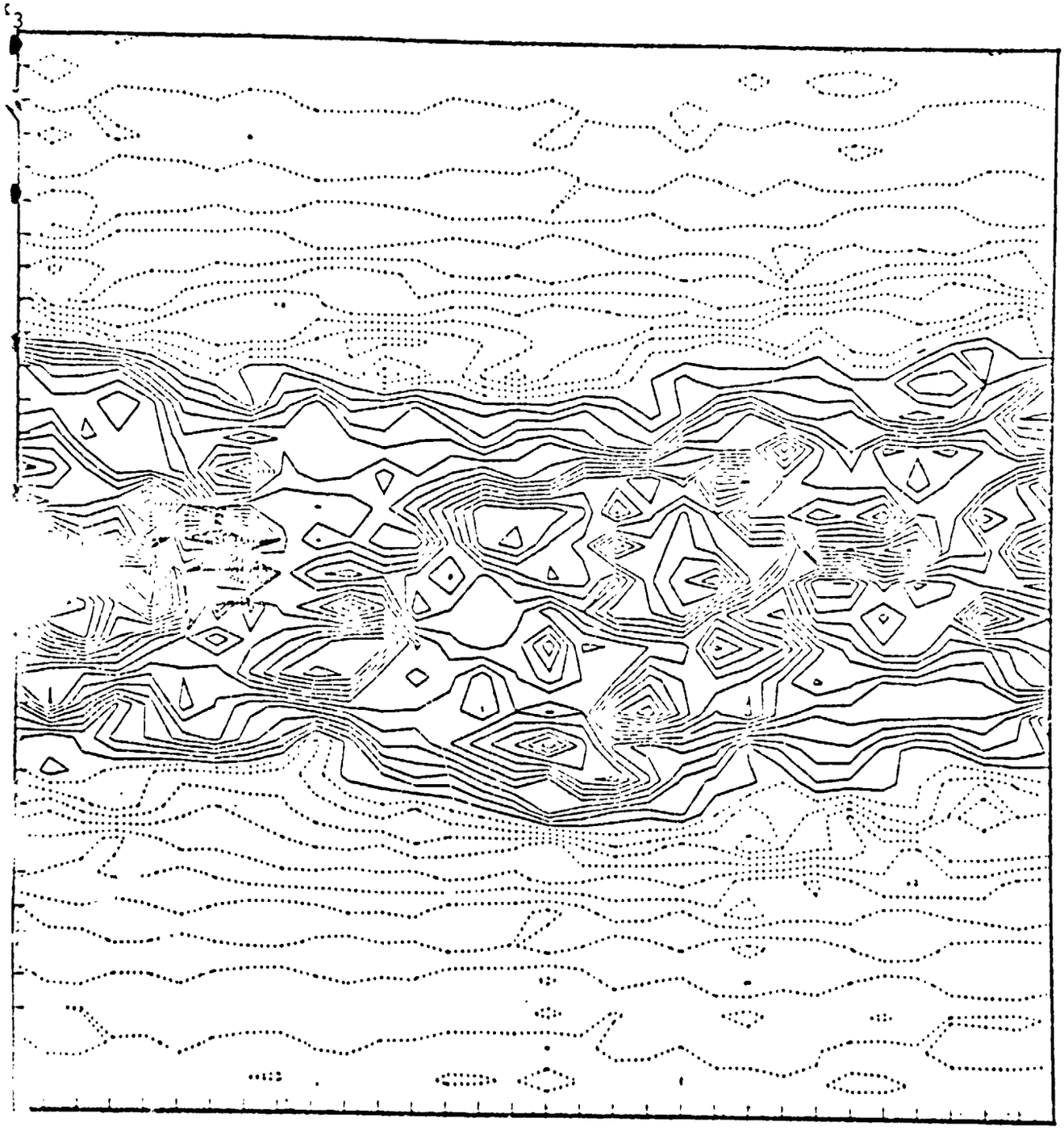

Figure 5. Contour plot of $v_1(x_1,x_2,x_3)$ in the plane $x_2=\frac{1}{2}L$ at $\bar{X}$=12 diameters downstream from the jet exit. Here t = .032s is the time of evolution.

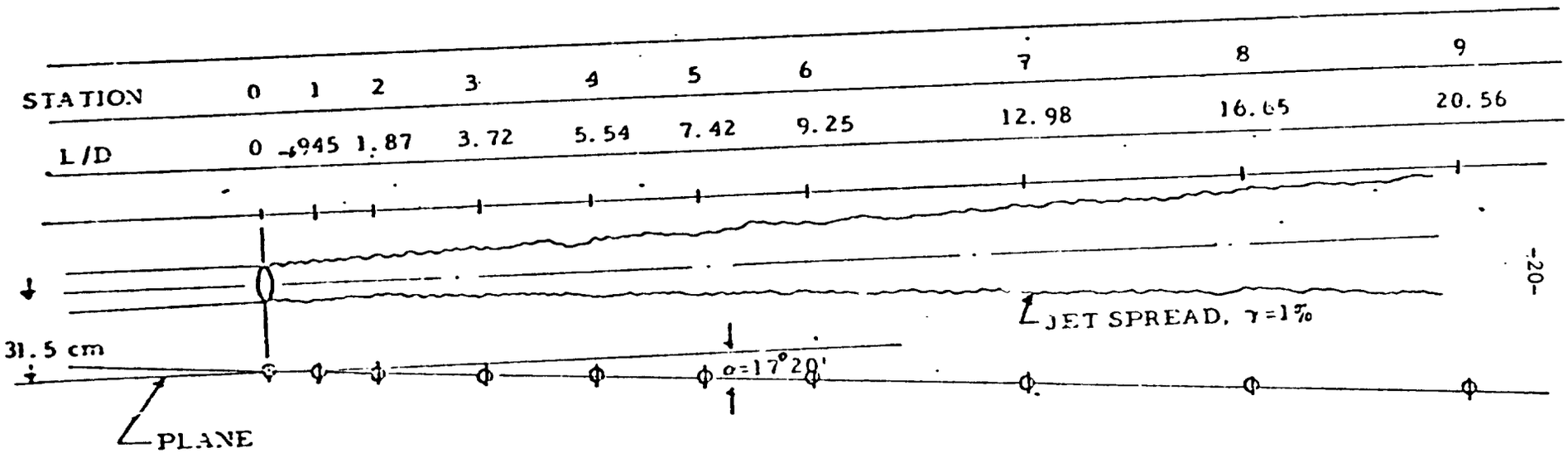

Figure 6. Geometry of Maestrello's(1973) experimental test setup. Our computations involve the simulation of the results of station 5 at 7.42 diameters downstream from the jet exit.

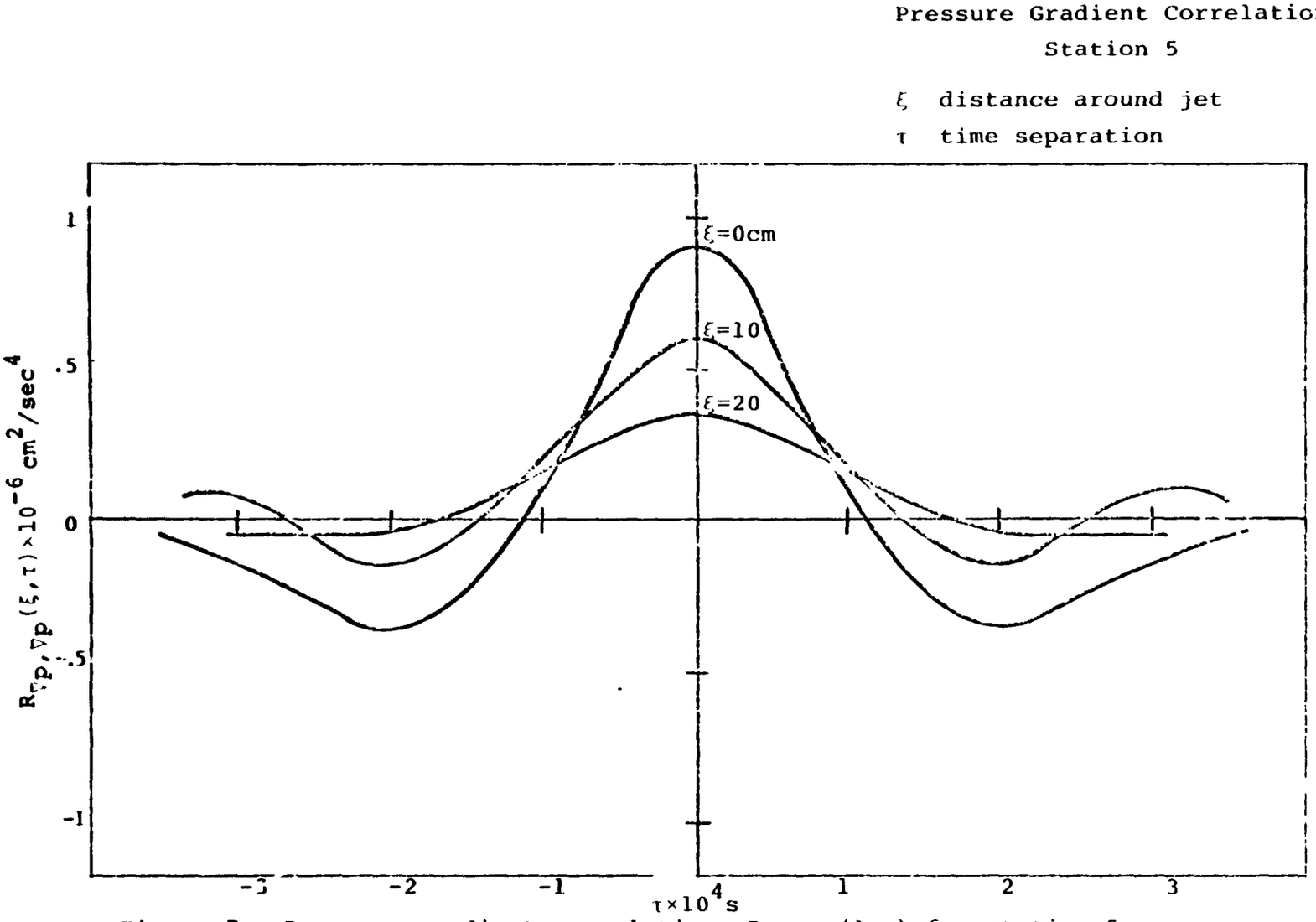

Figure 7. Pressure gradient correlation $R_{\nabla p,\nabla p}(\xi,\tau)$ for station 5 as a function of ξ and τ.

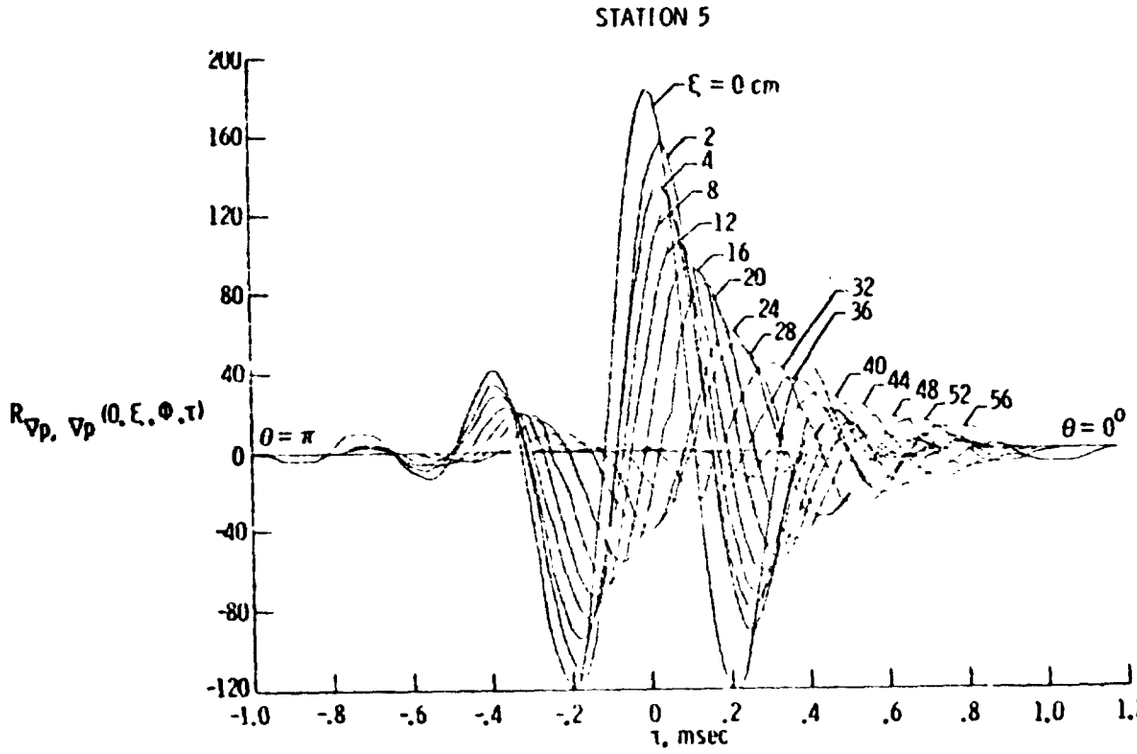

Figure 8. Broadband correlation of pressure gradient at station 5 as measured by Maestrello(1973).